IMA Journal of Applied Mathematics (2007) **72**, 865–893
doi:10.1093/imamat/hxm041
Advance Access publication November 1, 2007

Steric hindrance effects in thin reaction zones: applications to BIAcore

DAVID A. EDWARDS†
Department of Mathematical Sciences,
University of Delaware, Newark, DE 19716-2553, USA

[Received on 15 August 2006; revised on 27 July 2007]

Many biological and industrial processes have reactions which occur in thin zones of densely packed receptors. Understanding the rate of such reactions is important, and the BIAcore surface plasmon resonance biosensor for measuring rate constants has such a geometry. However, interpreting biosensor data correctly is difficult since large ligand molecules can block multiple receptor sites, thus skewing the kinetics. General mathematical principles are presented for handling this phenomenon, and a receptor layer model is presented explicitly. An integro-partial differential equation results. Using perturbation techniques, the problem can be simplified somewhat. In the limit of small Damköhler number, the non-local nature of the system becomes evident in the association problem, while other experiments can be modelled using local techniques. Explicit and asymptotic solutions are constructed for large-molecule cases motivated by experimental design. The analysis provides insight into surface–volume reactions occurring in various contexts. In particular, this steric hindrance effect can often be quantified with a single dimensionless parameter.

Keywords: biomolecular reactions; rate constants; asymptotics; integrodifferential equations; steric hindrance effects; BIAcore.

1. Introduction

Many biological and industrial processes include reactions in thin zones adjacent to a solid surface. In the simplest bimolecular model, one reactant (the 'ligand') floats free in solution, while the other (the 'receptor') is embedded in a thin 'reaction zone' (such as a gel) near the surface of a channel, cell membrane, etc.

Often the solution has an imposed flow. For instance, in bubble reactors, gas reacts with the liquid which impinges on the bubble surfaces (Long & Kalachev, 2000). The creation of alginate gel in the food industry is enhanced by the addition of a convective flow of reactant (Treml *et al.*, 2003). Flow reactors are more effective at synthesizing inorganic materials on templates (Mann *et al.*, 1997). In high-pressure, continuous-flow, fixed-bed reactors, gels are introduced at the reaction surface to minimize hydrodynamics effects (Jansen & Niemeyer, 2005). Harmful blood clots form when platelets adhere to foreign objects in the presence of blood flow (Grabowski *et al.*, 1972). Various biological processes ensue when ligands floating in the bloodstream bind to cell receptors which occupy a thin reaction zone about the cell membrane (Goldstein & Dembo, 1995). Immunoglobulins are transmitted to newborns from mother's milk through binding to receptors on intestinal epithelial cells (Raghavan *et al.*, 1994).

To control or understand such processes, one needs to know the 'rate constants' for any given reaction. If one can obtain real-time measurements of the binding process, these can be translated into such parameters given an appropriate mathematical model. One popular device for obtaining such data is the

†Email: edwards@math.udel.edu

BIAcore, which is a surface plasmon resonance (SPR) device, and for the purposes of this paper, we will use the BIAcore as a canonical example of a system where kinetics occur in a thin reaction zone.

The configuration of the BIAcore is described in great detail elsewhere (Karlsson & Fält, 1997; Karlsson *et al.*, 1991; Liedberg *et al.*, 1993; Szabo *et al.*, 1995). For our purposes, we consider the BIAcore to be a rectangular channel through which the ligand is convected in the $\tilde{x}$-direction in standard 2D laminar flow from $\tilde{x} = 0$, the inlet position (see Fig. 1). Receptors are embedded in a thin dextran gel of width H_g (where the subscript 'g' stands for 'gel') attached to the ceiling of the channel. An evanescent wave is bounced off the channel ceiling and read by a detector. As the experiment progresses, binding causes refractive changes to the polarized light beam. These changes, when compared to a control state, can be translated into a 'sensogram' of the binding (Garland, 1996).

Most models of the BIAcore to date have assumed that a single binding event will block only one receptor—the one to which the ligand molecule actually binds. However, in experiments the ligand molecule can be much larger than the receptors (Zheng & Rundell, 2003). In such cases, a single binding event can block multiple receptors (the 'steric hindrance effect'). A naive model which does not include the effect will underestimate the rate constant $\tilde{k}_a$ (where the subscript 'a' refers to 'association') because receptors which are merely occluded will be counted as receptors which are available, but do not bind because of the kinetics.

Edwards (2007) proposed a model where the reacting zone is treated as a surface (the limit $H_g \to 0$ in our terminology). In this work, we extend this model to include the case of a reacting zone of finite width. Alternatively, this can be seen as an extension of the work in Edwards (2001) to include occlusion effects. In Section 2, we present some general guidelines to observe when making such extensions. Using some reasonable assumptions, we then formulate an integro-partial differential equation for the concentration $\tilde{B}_g$ of the bound state. Though the integral term in the $\tilde{x}$-direction can be localized, in the $\tilde{y}$-direction it cannot and must be considered.

When the Damköhler number Da is small, we can obtain a perturbation solution to the problem for all time. Because of the external reservoir of ligand, in the association case the integral equation cannot be simplified, and we use standard solution techniques in the limit of large molecules. Without such an external reserve, the dissociation kinetics are much simpler.

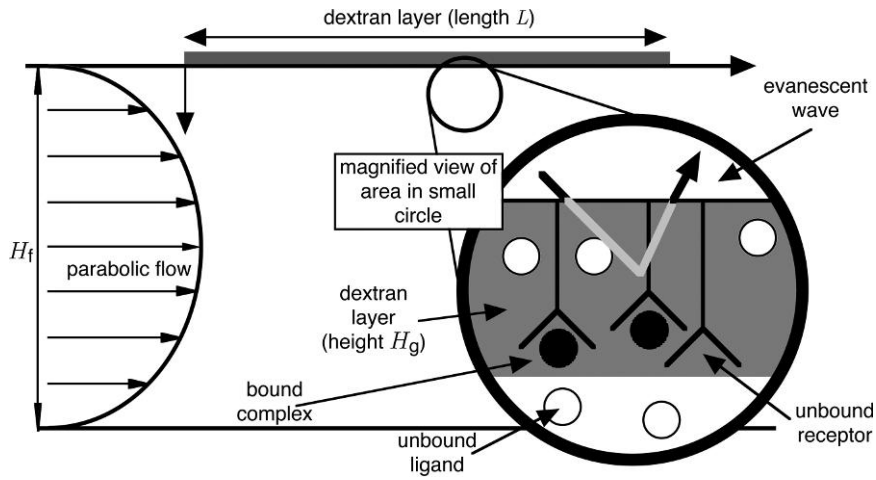

FIG. 1. Schematic of BIAcore device.

When $\mathrm{Da} = \mathrm{O}(1)$, only short-time solutions can be obtained. Again, since an external supply of ligand is not fully developed, both association and dissociation kinetics become straightforward extensions of the work in Edwards (2001, 2007). The changes occur only in certain dimensionless parameters in the problem. Such a simplification makes it easy to analyse, interpret and correct errors in the sensogram data due to steric hindrance effects.

The results presented herein for the BIAcore have wide applicability. The same occlusion effects can occur in biological contexts, and information about them can lead to the design of more effective pharmaceuticals. Such information can also help optimize industrial processes by providing upper bounds on the amount of receptor needed to achieve a certain chemical result.

2. The evolution equation

2.1 *General modelling*

We treat the reacting zone in the BIAcore as a thin dextran gel layer occupying the region $-H_\mathrm{g} \leqslant \tilde{y} \leqslant 0$. This is in contrast to the work in Edwards (2007), where the reacting zone is taken to be a surface. In the gel, the bound state is created when an available reacting site reacts with a ligand molecule (concentration $\tilde{C}_\mathrm{g}$). The bound state can also dissociate with rate constant $\tilde{k}_\mathrm{d}$ (where the subscript 'd' refers to 'dissociation'). Therefore, the mass balance equation becomes

$$\frac{\partial \tilde{B}_\mathrm{g}}{\partial \tilde{t}} = \tilde{k}_\mathrm{a} \left\{ \frac{R_\mathrm{T}}{H_\mathrm{g}} - \tilde{\mathcal{S}}[\tilde{B}_\mathrm{g}] \right\} \frac{\tilde{C}_\mathrm{g}(\tilde{x}, \tilde{y}, \tilde{t})}{\phi} - \tilde{k}_\mathrm{d} \tilde{B}_\mathrm{g}, \quad -H_\mathrm{g} \leqslant \tilde{y} \leqslant 0, \;\; 0 \leqslant \tilde{x} \leqslant L, \tag{2.1}$$

where L is the length of the channel. In addition:

1. Since the reaction occurs only inside the pores, it is the *fluid* concentration of $\tilde{C}_\mathrm{g}$ that is important in the reaction, so we must divide it by the partition coefficient ϕ.
2. The total number of (initially) available receptor sites R_T is usually expressed as an area concentration, so we must divide by the width of the gel to obtain a volume concentration.
3. The expression $\tilde{\mathcal{S}}[\tilde{B}_\mathrm{g}]$ represents the number of receptor sites occluded by the bound state at a particular point. Thus, the braced quantity represents the concentration of available (as opposed to unbound) receptors.

To specialize the general operator $\tilde{\mathcal{S}}$ to a form which we can actually solve, we make the following additional assumptions:

1. Receptor sites are considered to be points, spaced evenly in a cubic lattice in the dextran gel at a distance d_r from one another, where the subscript 'r' stands for 'receptor'.
2. Ligand molecules are considered to have only one specific binding site. (Generalizing our results to multiple binding sites is the subject of further research.) The structure is considered to be a solid sphere of characteristic size d_l, where the subscript 'l' stands for 'ligand'. In practice, d_l will be taken as twice the Stokes radius.
3. As the experiment progresses, molecules will form an optimal packing arrangement. This is probably the most controversial assumption, though in Section 2.2 we describe situations where this can occur. In any event, this assumption will provide a lower bound on the effect (since more disordered configurations will occlude more reacting sites).
4. In order to transition from discrete receptor sites on individual molecules to the continuum approximation in (2.1), we rely upon the fact that there is a third $\tilde{z}$-direction normal to the flow. All

the dependent variables are uniform in $\tilde{z}$ (Edwards, 2007), and hence $\tilde{B}_{\mathrm{g}}$ at some specified $\tilde{x}_*$ can be thought of as a proportion of receptor sites at $(\tilde{x}_*, \tilde{z})$ which have been bound, thus yielding after some manipulation a concentration.

If the diameter of the ligand molecule exceeds the receptor spacing, the ligand molecules will displace the receptors from their grid, as shown in Fig. 2. (This is possible because the dextran is a gel.) In addition, because the binding sites are on the surface of a sphere, it is possible for two receptors in close proximity to bind to separate ligand molecules. Note that this behaviour is not possible in the surface reaction case (Edwards, 2007).

These physical complications engender several mathematical ones. First, there is a question of how to track the dislocation of the receptor sites by the movement of the ligand sphere. Second, since we are going to embed this discrete system into a continuum model, we must decide how to identify the position of the ligand sphere. Fortunately, the BIAcore measures only the *spatial average* of the binding, not its exact *location*. (More details can be found in Section 3.1.) Therefore, any approximation without a directional bias should have errors that average to zero.

These two problems must be treated together. One obvious way to proceed would be to identify the position of the ligand molecule as its centre, and assume that the ligand molecule centres on the former position of a receptor molecule and binds to that molecule. However, as shown in Fig. 3, this would lead to ligand molecules 'above' the receptor layer participating in binding events, and receptors in the region $-H_{\mathrm{g}} \leqslant \tilde{y} < d_{\mathrm{l}}/2 - H_{\mathrm{g}}$ never being bound.

To solve these problems, we take the position of the binding site to be the lowest point on the sphere, as shown in Fig. 4. At left is a molecule dislodging receptors from their array. Binding to any of the white circles would be modelled by the diagram at right. (This effectively allows us to ignore rotational motion in the analysis.) Moreover, one should think of the case of a 2D reacting surface treated in Edwards (2007) to be the projection of the 3D reacting zone. Taking the receptor site to be the lowest point on the sphere allows our results to reduce to the 2D case (where the reacting site is centred on a disc) in the limit that $H_{\mathrm{g}} \to 0$.

As in the 2D case, spheres cannot overlap. Figure 5 shows that when binding occurs, it occludes all receptors within a sphere of radius d_{l} from the binding site. Receptors within a radius $d_{\mathrm{l}}/2$ are directly occluded by the ligand molecule, while receptors in the spherical annulus between radii $d_{\mathrm{l}}/2$ and d_{l} are unavailable because another ligand receptor cannot fit to bind.

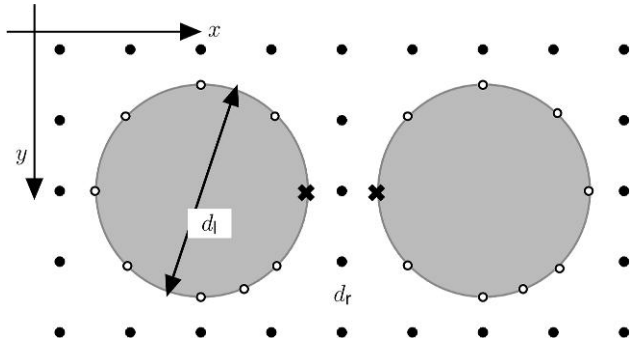

FIG. 2. 3D schematic of true physical situation, side view. An X represents the binding site; white circles represent dislodged receptor molecules.

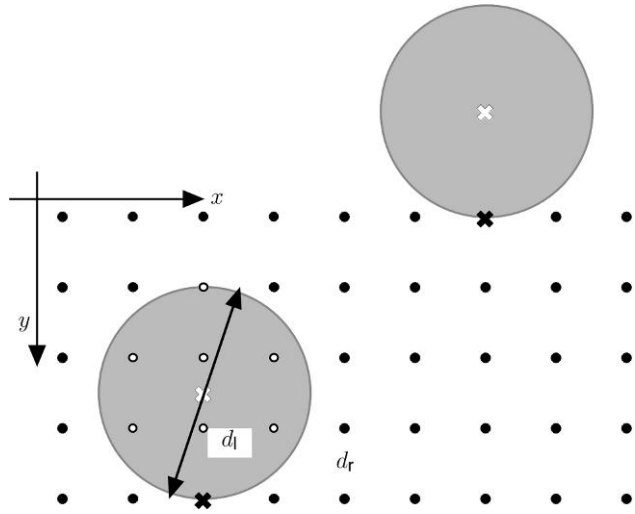

FIG. 3. 3D schematic of discredited mathematical approximation, side view. A black X represents the physical binding site, a white X represents the modelled binding site and white circles represent dislodged receptor molecules.

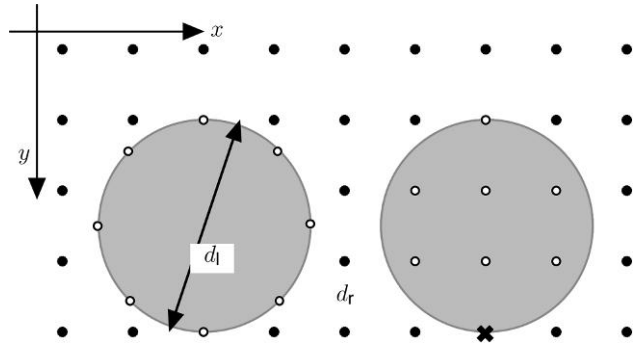

FIG. 4. 3D schematic of accepted mathematical approximation, side view. Left: true physical situation. Right: mathematical model.

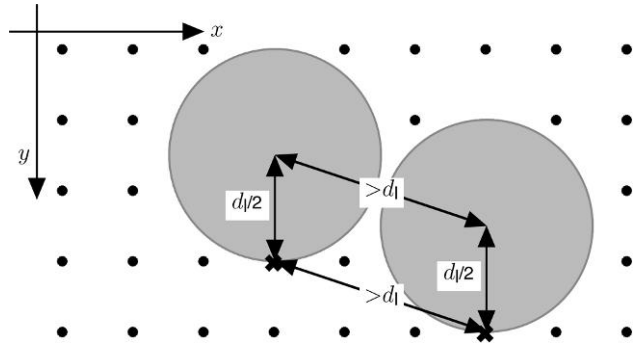

FIG. 5. Schematic of occlusion volume.

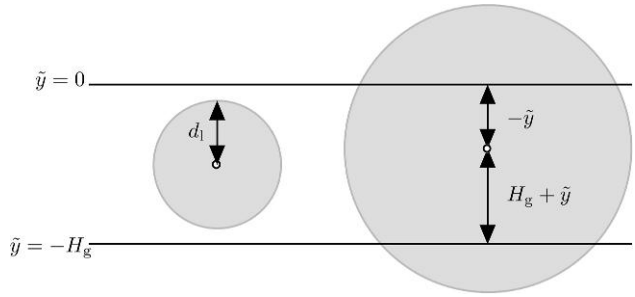

FIG. 6. Schematic of occlusion volume, side view.

This discussion motivates the following model for $\tilde{\mathcal{S}}$:

$$\tilde{\mathcal{S}}[\tilde{B}_g](\tilde{x}, \tilde{y}, \tilde{t}) = \mathcal{S}_0 \int_{-d_l}^{d_l} \int_{-\sqrt{d_l^2 - \tilde{y}'^2}}^{\sqrt{d_l^2 - \tilde{y}'^2}} 2\sqrt{d_l^2 - \tilde{x}'^2 - \tilde{y}'^2}\, \tilde{B}_g(\tilde{x} + \tilde{x}', \tilde{y} + \tilde{y}', \tilde{t}) \mathrm{d}\tilde{x}'\, \mathrm{d}\tilde{y}', \tag{2.2}$$

where $\mathcal{S}_0$ is a normalization factor. Physically, (2.2) just says that the availability of a binding site is dependent on the bound state in a ball of radius d_l, which corresponds exactly with the graphical interpretation in Fig. 5.

Note from (2.2) that the occlusion volume (and hence the range of integration of $\tilde{y}$) may extend outside the receptor layer, as shown in Fig. 6. Thus, when using (2.2), one must keep in mind that $\tilde{B}_g \equiv 0$ outside this interval. Alternatively, we adjust the $\tilde{y}'$-limits of integration for the integral as follows.

On the left of Fig. 6 is shown an event with a position and radius such that the occlusion volume resides entirely in the receptor layer. In such a situation, (2.2) may be used without change. However, on the right is an event where the occlusion volume protrudes beyond the receptor layer. In such an instance, the limits of integration would be $-\tilde{y}$ and $-(H_g + \tilde{y})$. (Note that due to the form of (2.2), the range of integration corresponds to *signed distance*, not $\tilde{y}$-value.)

In general, (2.2) may be written as

$$\tilde{\mathcal{S}}[\tilde{B}_g](\tilde{x}, \tilde{y}, \tilde{t}) = \mathcal{S}_0 \int_{\tilde{y}_{\min}}^{\tilde{y}_{\max}} \int_{-\sqrt{d_l^2 - \tilde{y}'^2}}^{\sqrt{d_l^2 - \tilde{y}'^2}} 2\sqrt{d_l^2 - \tilde{x}'^2 - \tilde{y}'^2}\, \tilde{B}_g(\tilde{x} + \tilde{x}', \tilde{y} + \tilde{y}', \tilde{t}) \mathrm{d}\tilde{x}'\, \mathrm{d}\tilde{y}', \tag{2.3a}$$

$$\tilde{y}_{\min} = -\min\{d_l, H_g + \tilde{y}\}, \quad \tilde{y}_{\max} = \min\{d_l, -\tilde{y}\}. \tag{2.3b}$$

2.2 *Scaling and normalization*

To simplify the calculations, we introduce dimensionless variables into the equations. For the physical variables, we use scalings motivated by Edwards (2001). In particular, we normalize $\tilde{x}$ by the channel

length, $\tilde{y}$ by the width of the receptor layer, $\tilde{t}$ by the forward reaction timescale and the bound state by the initial receptor density. Thus, we have

$$x = \frac{\tilde{x}}{L}, \quad y = \frac{\tilde{y}}{H_g}, \quad t = \tilde{k}_a C_u \tilde{t}, \quad B_g(x, y, t) = \frac{\tilde{B}_g(\tilde{x}, \tilde{y}, \tilde{t})}{R_T/H_g}, \tag{2.4a}$$

$$\mathcal{S}[B_g] = \frac{\tilde{\mathcal{S}}[\tilde{B}_g]}{R_T/H_g}, \quad \tilde{C}_g(\tilde{x}, \tilde{y}, \tilde{t}) = \phi C_u[1 - \mathrm{Da} C_g(x, y, t)], \tag{2.4b}$$

where C_u is the upstream inlet concentration. Here, Da is the 'Damköhler number', given by

$$\mathrm{Da} = \frac{\tilde{k}_a R_T}{\tilde{D}_f/(H_f \mathrm{Pe}^{-1/3})} = \frac{\text{reaction 'velocity'}}{\text{diffusion 'velocity' in diffusive boundary layer}}, \tag{2.5a}$$

where $\tilde{D}_f$ is the diffusion coefficient of the ligand molecules in the flow (which the subscript 'f' represents), H_f is the height of the channel and Pe is the Péclet number, given by

$$\mathrm{Pe} = \frac{H_f^2/\tilde{D}_f}{L/V} = \frac{\text{characteristic diffusion time in flow}}{\text{characteristic convection time in flow}}, \tag{2.5b}$$

where V is a typical velocity scale. The importance of the scaling is that the dimensionless B_g now represents the percentage of receptor sites bound.

Note from (2.4b) that the dimensionless C_g is a scaled displacement of $\tilde{C}_g$ from its equilibrium value. In many experiments, Da is a small parameter (see Sections 4–6), and hence C_g can be interpreted as the first term in a perturbation series. However, even in the case where $\mathrm{Da} = \mathrm{O}(1)$ (see Section 7), this choice of scaling simplifies the algebra later on.

Substituting (2.4) into (2.1), we have the following:

$$\frac{\partial B_g}{\partial t} = \{1 - \mathcal{S}[B_g]\}[1 - \mathrm{Da} C_g(x, y, t)] - K B_g, \quad K = \frac{\tilde{k}_d}{\tilde{k}_a C_u}. \tag{2.6}$$

For the dummy variables in (2.3a), it is more convenient to scale by d_l:

$$x' = \frac{\tilde{x}'}{d_l}, \quad y' = \frac{\tilde{y}'}{d_l}. \tag{2.7}$$

Substituting (2.4) and (2.7) into (2.3a), we obtain

$$\mathcal{S}[B_g](x, y, t) = 2\mathcal{S}_0 d_l^3 \int_{y_{\min}}^{y_{\max}} \int_{-\sqrt{1-y'^2}}^{\sqrt{1-y'^2}} \sqrt{1 - x'^2 - y'^2}\, B_g(x + \delta_x x', y + \delta_y y', t) \mathrm{d}x' \, \mathrm{d}y', \tag{2.8}$$

$$\delta_x = \frac{d_l}{L}, \quad \delta_y = d_l H_g, \tag{2.9a}$$

$$y_{\min} = -\min\{1, \delta_y^{-1}(1 + y)\}, \quad y_{\max} = \min\{1, -\delta_y^{-1} y\}. \tag{2.9b}$$

To calculate $\mathcal{S}_0$, we consider a nearly irreversible reaction by taking $K \to 0$. Physically, we are saying that the backwards reaction proceeds slowly. Rather than affecting the chemistry, the back reaction

eliminates poorly packed configurations, working only to distribute the bound state uniformly. It will be shown in Section 6 that the steady state of C_g is zero.

Thus, in the small-K limit, the steady state of (2.6) becomes

$$2\mathcal{S}_0 d_l^3 \int_{y_{\min}}^{y_{\max}} \int_{-\sqrt{1-y'^2}}^{\sqrt{1-y'^2}} \sqrt{1-x'^2-y'^2}\, B_{g,s}(x+\delta_x x', y+\delta_y y')\mathrm{d}x'\,\mathrm{d}y' = 1, \tag{2.10}$$

where the subscript 's' refers to 'steady state'. Physically, (2.10) states that for a nearly irreversible reaction at steady state, all the receptors must be either bound or occluded.

In the continuous limit of averaging with perfect distribution of binding sites, $B_{g,s}$ will be uniform. Examining the schematic in Fig. 7, where $d_l \approx 2d_r$, we see that each ligand occludes eight receptors (neglecting edge effects and considering that the ligands are spheres). Thus, only 1/8 of the receptors will ever be bound even if the discs were packed optimally. Similarly, as long as $d_l \geqslant d_r$, the proportion of receptors bound at steady state is given by $(d_r/d_l)^3$. Essentially, we say that a spherical ligand blocks out all receptors in the cube in which it resides.

This analysis assumes that $d_l < H_g$. Otherwise, the size of the 'box' that the receptor will block is $d_l^2 H_g$ since its height must be given by the width of the receptor layer, not d_l. Therefore, in this case the steady state is given by

$$B_{g,s} = \frac{d_r^3}{d_l^2 \min\{d_l, H_g\}}, \tag{2.11}$$

as long as the receptors are spaced more closely than the ligand diameter. If they are not, then the concentration of the bound state is trivially equal to 1.

It is simpler algebraically to work with the inverse of this quantity, which we denote by p. (Note that this is a slightly different notation from Edwards (2007), where the analogous quantity is called p^2.) Thus, we have

$$p = \max\left\{\frac{d_l^2 \min\{d_l, H_g\}}{d_r^3}, 1\right\}, \tag{2.12}$$

where we use the maximum to take into account the case where the ligand size is smaller than the receptor spacing.

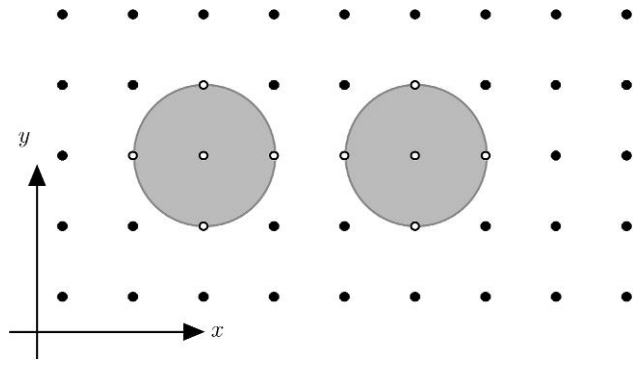

FIG. 7. Packing with $d_l = 2d_r$, side view.

There may be some concern about the validity of (2.12) because it would seem to ignore various aspects of geometry, packing, etc. that could affect our results. We present a brief discussion to assuage those concerns by examining the special case where $d_l = d_r$. Then, a typical packing is shown in Fig. 8. Note that the fraction of the *volume* covered by the spheres is $\pi/6$ (since we are working in three dimensions), while the fraction of the *receptors* covered by the spheres is 1. In general, since the receptors are assumed to occupy a cubic lattice, we have the following:

$$B_{g,s} = \frac{6}{\pi} \text{volume fraction} = \frac{6}{\pi} \frac{\pi d_l^3/6}{d_r^3} = p^{-1},$$

as desired.

In order to apply our theory to a particular experiment, we must know the value of p. d_l is readily obtainable from the Stokes radius for the ligand molecule, which can be estimated using gel filtration techniques (Gherardi *et al.*, 2003) or size exclusion chromatography (Sutovsky & Gazit, 2004). The volume density of receptors is given by dividing the area density $N R_T$ by H_g, where N is Avogadro's number. (Note that this implies closer packing as $H_g \to 0$.) Thus, in the case where $d_l > d_r$, we have that

$$p = \frac{d_l^2 \min\{d_l, H_g\}}{d_r^3} = \frac{\text{volume density of receptors}}{\text{volume density of ligands in } \textit{receptor layer}} = d_l^2 \min\{\delta_y, 1\} N R_T. \quad (2.13)$$

Since p is directly proportional to R_T, it can be controlled in an experiment.

With $B_{g,s}$ a constant, the integral in (2.10) is easily computed, and we find

$$\mathcal{S}_0(y; d_l) = \frac{p}{\pi d_l^3} \left\{ \left[y' - \frac{y'^3}{3} \right]_{y_{min}}^{y_{max}} \right\}^{-1}, \quad (2.14)$$

where we explicitly list the dependence of $\mathcal{S}_0$ on y (and its parametric dependence on d_l). The normalization factor is not a constant since it is related to the volume of the occluded region in the receptor layer, which is cut off as y approaches the boundaries of the layer. Note also from (2.8) that with the choice of $\mathcal{S}_0$ in (2.14),

$$\mathcal{S}[B_*] = p B_* \text{ for any } B_* \text{ independent of } y. \quad (2.15)$$

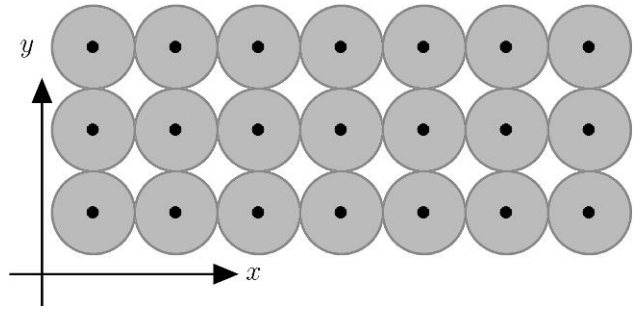

FIG. 8. Packing with $d_l = d_r$, side view.

2.3 *Reduction to previous cases*

In order to verify our results, we show that they reduce to previous cases in various physically meaningful limits. In the limit as $d_\mathrm{l} \to 0$, our results should match those in a receptor layer neglecting occlusion. In this limit,

$$\delta_x = 0, \quad \delta_y = 0, \quad y_\mathrm{min} = -1, \quad y_\mathrm{max} = 1, \quad p = 1, \quad \mathcal{S}_0 = \frac{3}{4\pi d_\mathrm{l}^3}. \tag{2.16}$$

Substituting (2.16) into (2.8), we obtain

$$\begin{aligned}\lim_{d_\mathrm{l}\to 0} \mathcal{S}[B_\mathrm{g}](x,y,t) &= \lim_{d_\mathrm{l}\to 0} 2\left(\frac{3}{4\pi d_\mathrm{l}^3}\right) d_\mathrm{l}^3 \int_{-1}^{1}\int_{-\sqrt{1-y'^2}}^{\sqrt{1-y'^2}} \sqrt{1-x'^2-y'^2}\, B_\mathrm{g}(x,y,t)\mathrm{d}x'\,\mathrm{d}y' \\ &= B_\mathrm{g}(x,y,t),\end{aligned}$$

which is of course the desired result because without occlusion, $\mathcal{S}[B_\mathrm{g}] = B_\mathrm{g}$.

In the limit that $H_\mathrm{g} \to 0$, our results should reduce to the 2D result in Edwards (2007) with occlusion included. We first note that if $\tilde{B}^{(2)}$ is the bound concentration in the 2D case mentioned in Edwards (2007), then

$$\tilde{B}^{(2)}(\tilde{x},\tilde{t}) = \int_{-H_\mathrm{g}}^{0} \tilde{B}_\mathrm{g}(\tilde{x},\tilde{y},\tilde{t})\mathrm{d}\tilde{y}. \tag{2.17}$$

Introducing the same averaging into (2.1) yields

$$\frac{\partial \tilde{B}^{(2)}}{\partial \tilde{t}} = \frac{\tilde{k}_\mathrm{a}}{\phi}\left\{ R_\mathrm{T}\tilde{C}_\mathrm{g}(\tilde{x},0,\tilde{t}) - \lim_{H_\mathrm{g}\to 0}\int_{-H_\mathrm{g}}^{0} \tilde{\mathcal{S}}[\tilde{B}_\mathrm{g}]\tilde{C}_\mathrm{g}\,\mathrm{d}\tilde{y}\right\} - \tilde{k}_\mathrm{d}\tilde{B}^{(2)}, \tag{2.18}$$

where we have used the Mean Value Theorem.

Also in the limit that $H_\mathrm{g} \to 0$, we have that

$$\begin{aligned}&\delta_y \to \infty, \quad y_\mathrm{min} = -\delta_y^{-1}(1+y), \quad y_\mathrm{max} = -\delta_y^{-1}y, \\ &\qquad \tilde{y}_\mathrm{min} = -(H_\mathrm{g}+\tilde{y}), \quad \tilde{y}_\mathrm{max} = -\tilde{y}, \quad p = d_\mathrm{l}^2 N R_\mathrm{T},\end{aligned} \tag{2.19a}$$

$$\lim_{H_\mathrm{g}\to 0}\mathcal{S}_0 = \lim_{H_\mathrm{g}\to 0}\frac{1}{\pi d_\mathrm{l}^3} d_\mathrm{l}^2 N R_\mathrm{T}\left\{\left[y' - \frac{y'^3}{3}\right]_{-\delta_y^{-1}(1+y)}^{-\delta_y^{-1}y}\right\}^{-1} = \frac{p^{(2)}}{\pi d_\mathrm{l}^2}\lim_{H_\mathrm{g}\to 0}\frac{1}{H_\mathrm{g}}, \tag{2.19b}$$

where $p^{(2)}$ is the 2D analog of our normalization factor p.

Substituting (2.19) into (2.3a), we obtain

$$\lim_{H_\mathrm{g}\to 0}\int_{-H_\mathrm{g}}^{0} \tilde{\mathcal{S}}[\tilde{B}_\mathrm{g}]\tilde{C}_\mathrm{g}\,\mathrm{d}\tilde{y} = \frac{2p^{(2)}R_\mathrm{T}}{\pi}\int_{-1}^{1}\sqrt{1-x'^2}\,B^{(2)}(x+\delta_x x',t)\mathrm{d}x'\tilde{C}_\mathrm{g}(\tilde{x},0,\tilde{t}), \tag{2.20}$$

where we have used the Mean Value Theorem and the fact that the scaling in the 2D case is $\tilde{B}^{(2)} = R_\mathrm{T}B^{(2)}$ (Edwards, 2007). Moreover, with the partition coefficient included, continuity of concentration

at the flow–dextran interface is given by $\phi\tilde{C}_{\rm f}(\tilde{x},0,\tilde{t})=\tilde{C}_{\rm d}(\tilde{x},0,\tilde{t})$. Using this fact and (2.20) in (2.18), we find that

$$\frac{\partial B^{(2)}}{\partial t}=\left[1-\frac{2p^{(2)}}{\pi}\int_{-1}^{1}\sqrt{1-x'^2}B^{(2)}(x+\delta_x x',t)\mathrm{d}x'\right][1-\mathrm{Da}C_{\rm f}(x,0,t)]-KB^{(2)}, \tag{2.21}$$

where we have used the scaling for $C_{\rm f}$ in Edwards (2007). Equation (2.21) exactly matches the analogous result in that work, with our $p^{(2)}$ being denoted as p^2.

3. Additional equations

3.1 *The bound state*

Since (2.6) is an evolution equation, we need an initial condition for $B_{\rm g}$. In the experiments under consideration, it is appropriate to use a constant initial condition

$$B_{\rm g}(x,y,0)=B_{\rm i}. \tag{3.1}$$

In the BIAcore, it is not the actual value of $B_{\rm g}$ which is calculated, but rather its average over some 'scanning range' $x_{\min}\leqslant x\leqslant x_{\max}$ and the width of the receptor layer. Denoting that quantity with a bar, we have

$$\bar{B}_{\rm g}(t)=\frac{1}{x_{\max}-x_{\min}}\int_{x_{\min}}^{x_{\max}}\langle B_{\rm g}\rangle\mathrm{d}x,\quad \langle B_{\rm g}\rangle=\int_{-1}^{0}B_{\rm g}\,\mathrm{d}y. \tag{3.2}$$

Lastly, we may simplify our expressions using experimentally appropriate parameter regimes. It can be shown (Edwards, 2007) that $\delta_x\ll 1$. Thus, expanding the inner integral term in (2.8) for small δ_x, we obtain

$$\mathcal{S}[B_{\rm g}](x,y,t)=2\mathcal{S}_0 d_{\rm l}^3\int_{y_{\min}}^{y_{\max}}\frac{\pi(1-y'^2)}{2}\left[B_{\rm g}+\frac{\delta_x^2(1-y'^2)}{8}\frac{\partial^2 B_{\rm g}}{\partial x^2}\right](x,y+\delta_y y',t)\mathrm{d}y'. \tag{3.3}$$

3.2 *Free ligand*

To complete the system, we need an expression for $C_{\rm g}$. With our scalings, the balance is between diffusion of $C_{\rm g}$ and the reaction, so we have (Edwards, 2001)

$$\frac{\partial^2 C_{\rm g}}{\partial y^2}=-D\frac{\partial B_{\rm g}}{\partial t},$$

$$D=\frac{\tilde{D}_{\rm f}/(H_{\rm f}\mathrm{Pe}^{-1/3})}{\phi\tilde{D}_{\rm g}/H_{\rm g}}=\frac{\text{diffusion 'velocity' in diffusive boundary layer}}{\text{diffusion 'velocity' in dextran}}, \tag{3.4}$$

where $\tilde{D}_{\rm g}$ is the diffusion coefficient in the dextran gel. Following the analysis in Edwards (2001), if we now define

$$\frac{\partial^2 F_y}{\partial y^2}=\frac{\partial B_{\rm g}}{\partial t},\quad \frac{\partial F_y}{\partial y}(x,-1,t)=0,\quad F_y(x,0,t)=0, \tag{3.5}$$

then C_g is given by

$$C_g(x, y, t) = -[DF_y + F_x(x, t)], \tag{3.6}$$

$$F_x(x, t) = -\frac{1}{3^{1/3}\Gamma(2/3)} \int_0^x \frac{\partial F_y}{\partial y}(x - \xi, 0, t) \frac{d\xi}{\xi^{2/3}}. \tag{3.7}$$

Note from (3.5) that

$$\frac{\partial F_y}{\partial y}(x, 0, t) = \left\langle \frac{\partial B_g}{\partial t} \right\rangle, \tag{3.8}$$

where we have used the no-flux boundary condition. Hence, F_x represents the average depletion upstream due to the reaction.

Substituting (3.6) into (2.6), we obtain

$$\frac{\partial B_g}{\partial t} = \{1 - \mathcal{S}[B_g]\}[1 + \mathrm{Da}(DF_y + F_x)] - K B_g. \tag{3.9}$$

4. Small Da

In order to minimize the effects of transport, experimentalists attempt to force $\mathrm{Da} \ll 1$. Thus, we treat it as a small parameter and introduce a standard perturbation series

$$B_g(x, y, t) = B_0(x, y, t) + \mathrm{Da} B_1(x, y, t) + o(\mathrm{Da}). \tag{4.1}$$

Substituting (4.1) into (3.9), (3.5) and (3.1) while keeping the necessary orders, we have

$$\frac{\partial B_0}{\partial t} = \left\{1 - \pi \mathcal{S}_0 d_1^3 \int_{y_{\min}}^{y_{\max}} (1 - y'^2) B_0(x, y + \delta_y y', t) dy'\right\} - K B_0, \tag{4.2a}$$

$$\begin{aligned}\frac{\partial B_1}{\partial t} = {} & \left\{1 - \pi \mathcal{S}_0 d_1^3 \int_{y_{\min}}^{y_{\max}} (1 - y'^2) B_0(x, y + \delta_y y', t) dy'\right\} (DF_y + F_x) \\ & - \pi \mathcal{S}_0 d_1^3 \int_{y_{\min}}^{y_{\max}} (1 - y'^2) \left[B_1 + \frac{\delta_x^2 (1 - y'^2)}{8\mathrm{Da}} \frac{\partial^2 B_0}{\partial x^2}\right](x, y + \delta_y y', t) dy' - K B_1,\end{aligned} \tag{4.2b}$$

$$\frac{\partial^2 F_y}{\partial y^2} = \frac{\partial B_0}{\partial t}, \quad \frac{\partial F_y}{\partial y}(x, -1, t) = 0, \quad F_y(x, 0, t) = 0, \tag{4.3}$$

$$B_0(x, y, 0) = B_i, \quad B_1(x, y, 0) = 0. \tag{4.4}$$

Note from (4.2b) that we have assumed that $\delta_x^2 = O(\mathrm{Da})$.

It can be easily shown using (2.15) that $B_0 = B_0(t)$ satisfies (4.2a), which becomes

$$\frac{dB_0}{dt} + \alpha B_0 = 1, \quad \alpha = K + p. \tag{4.5}$$

The only difference between (4.5) and the receptor layer work in Edwards (2001) without occlusion is the redefinition of the parameter α. Note also that in the limit that $d_l \to 0$, $p \to 1$ and we reduce exactly to the results in Edwards (2001). Since this is the only change at leading order, it is easy to interpret how neglecting steric hindrance can affect our results. In particular, if we ignore steric hindrance effects when analysing our data, then the estimated value deviates from the true value in the following way:

$$K_{\text{estimated}} = K_{\text{true}} + p - 1. \tag{4.6}$$

Therefore, the error will be most apparent when K_{true} is small. Since the dimensionless parameter K depends on the underlying flow rate C_u (as shown in (2.6)), this error is controllable in a physical experiment even if the diameter of the ligand molecule is unknown.

The solution of (4.5) and (4.4) is given by

$$B_0(x,t) = \frac{1-\mathrm{e}^{-\alpha t}}{\alpha} + B_i\,\mathrm{e}^{-\alpha t} = \bar{B}_0(t). \tag{4.7}$$

Since B_0 is independent of x and y, the dependence of C_g on the various independent variables separates. In particular, the solution of (4.3) is

$$F_y(y,t) = \frac{\mathrm{d}B_0}{\mathrm{d}t}\frac{y(y+2)}{2}, \tag{4.8a}$$

which is independent of x, and F_x becomes

$$F_x(x,t) = -h(x)\frac{\mathrm{d}B_0}{\mathrm{d}t}, \quad h(x) = \frac{3^{2/3}x^{1/3}}{\Gamma(2/3)}, \tag{4.8b}$$

where we have used (3.7). Thus, F_x is independent of y. This decoupling of x- and y-transport processes also occurs in the receptor layer model without occlusion (Edwards, 2001).

Substituting (4.8) and the fact that B_0 depends only on t into (4.2b), we obtain

$$\frac{\partial B_1}{\partial t} + KB_1 = [1-pB_0(t)]\frac{\mathrm{d}B_0}{\mathrm{d}t}\left[D\frac{y(y+2)}{2} - h(x)\right] - \pi\mathcal{S}_0 d_l^3 \int_{y_{\min}}^{y_{\max}} (1-y'^2)B_1(x, y+\delta_y y', t)\mathrm{d}y', \tag{4.9}$$

where we have used (2.15). (Note that since B_0 is independent of y, the term involving δ_x^2 does not appear.) We may continue to exploit the structure to separate variables by defining

$$B_1(x,y,t) = B_x(x,t) + B_y(y,t), \quad B_x(x,0) = 0, \quad B_y(y,0) = 0. \tag{4.10}$$

Then, by using (2.15), we see that the evolution equation for B_x is

$$\frac{\partial B_x}{\partial t} + KB_x = -[1-pB_0(t)]\frac{\mathrm{d}B_0}{\mathrm{d}t}h(x) - pB_x,$$

and the solution is given by

$$B_x(x,t) = \left[\frac{(\mathrm{e}^{-\alpha t}-1)p\chi}{\alpha} - Kt\right]\frac{\chi\,\mathrm{e}^{-\alpha t}h(x)}{\alpha}, \quad \chi = 1-\alpha B_i, \tag{4.11}$$

where we have used (4.10).

Because of the integral term, the solution for B_y is more involved, as can be seen from its evolution equation

$$\frac{\partial B_y}{\partial t}+K B_y = \frac{D\chi}{\alpha}(K+p\chi\,\mathrm{e}^{-\alpha t})\mathrm{e}^{-\alpha t}\left[\frac{y(y+2)}{2}\right]-\pi\mathcal{S}_0 d_\mathrm{l}^3\int_{y_\mathrm{min}}^{y_\mathrm{max}}(1-y'^2)B_y(y+\delta_y y',t)\mathrm{d}y'. \quad (4.12)$$

First, we introduce the standard concept of a Laplace transform in the t-direction, as well as an intermediate variable $Y(y)$:

$$\hat{f}(s)=\int_0^\infty f(t)\mathrm{e}^{-st}\,\mathrm{d}t, \quad f(t)=\frac{1}{2\pi\,\mathrm{i}}\int_{\mathcal{C}}\hat{f}(s)\mathrm{e}^{st}\,\mathrm{d}s,$$

$$\hat{B}_y=\frac{D\chi}{2\alpha}\left(\frac{K}{s+\alpha}+\frac{p\chi}{s+2\alpha}\right)Y(y), \quad (4.13)$$

where $\mathcal{C}$ is the Bromwich contour. Substituting (4.13) into the Laplace transform of (4.12), we obtain

$$Y(s+K)=y(y+2)-\frac{\pi\mathcal{S}_0 d_\mathrm{l}^3}{\delta_y}\int_{\xi_\mathrm{min}}^{\xi_\mathrm{max}}\left[1-\left(\frac{\xi-y}{\delta_y}\right)^2\right]Y(\xi)\mathrm{d}\xi, \quad (4.14a)$$

$$\xi_\mathrm{min}=\max\{y-\delta_y,-1\}, \quad \xi_\mathrm{max}=\min\{y+\delta_y,0\}, \quad (4.14b)$$

where we have introduced the variable substitution $\xi=y+\delta_y y'$ for simplicity. Note that the kernel is both separable (useful for the Fredholm case) and a function of $y-\xi$ (useful for the Volterra case).

5. Large molecule limit, small Da

5.1 *Association experiment*

For the purposes of the rest of this manuscript, we focus on the case where $\delta_y > 1$, namely, those cases where the ligand molecule is larger than the dextran layer. (Such a regime is experimentally realizable; see the Appendix.) Since $-1 \leqslant y \leqslant 0$, we can calculate the value of $\mathcal{S}_0$ using (2.9b):

$$\mathcal{S}_0^{-1}(y;d_\mathrm{l})=-\frac{\pi d_\mathrm{l}^3}{p\delta_y^3}A(y), \quad A(y)=\frac{(2y+1)^2-r^2}{4}, \quad r^2=4\delta_y^2-\frac{1}{3}. \quad (5.1)$$

From (4.14b), we have that $\xi_\mathrm{min}=-1$ and $\xi_\mathrm{max}=0$, and hence (4.14a) becomes

$$Y(s+K)=y(y+2)+\frac{p}{A(y)}[(\delta_y^2-y^2)Y_0+2yY_1-Y_2], \quad Y_j=\langle y^j Y\rangle, \quad (5.2)$$

where we have used (5.1). Here, Y_j is the integral of $Y(y)$ against a test function y^j.

Equation (5.2) is now in a standard Fredholm form with separable kernel. Thus, to solve for the Y_j, we next take the inner product of the whole equation with a test function y^j, $j=0,1,2$. If we define

$$A_j=\left\langle\frac{y^j}{A(y)}\right\rangle, \quad j=0,1,\ldots,4, \quad (5.3)$$

then by symmetry arguments, all the A_j may be expressed as affine functions of

$$A_0=\frac{2}{r}\log\left(\frac{r-1}{r+1}\right). \quad (5.4)$$

Integrating (5.2) against the test functions, we have the following linear system of equations in the Y_j:

$$(s+K)Y_0 = -\frac{2}{3} - p\left[\left(1+\frac{A_0}{6}\right)Y_0 + A_0Y_1 + A_0Y_2\right], \tag{5.5a}$$

$$(s+K)Y_1 = \frac{5}{12} + p\left\{\left(\frac{3}{2}+\delta_y^2 A_0\right)Y_0 + 2\left[1+\left(\delta_y^2+\frac{1}{6}\right)A_0\right]Y_1 + \frac{A_0}{2}Y_2\right\}, \tag{5.5b}$$

$$\begin{aligned}(s+K)Y_2 = &-\frac{3}{10} - p\left\{\left[3+\left(\frac{7\delta_y^2}{3}-\frac{1}{9}\right)\frac{A_0}{2}\right]Y_0 + 3(1+\delta_y^2A_0)Y_1\right.\\ &\left.-\left[1+\left(\delta_y^2+\frac{1}{6}\right)A_0\right]Y_2\right\}.\end{aligned} \tag{5.5c}$$

We note that due to the averaging properties of the BIAcore, we need only the following quantity to compare to the sensogram signal:

$$\langle \hat{B}_y\rangle = \frac{D\chi}{2\alpha}\left(\frac{K}{s+\alpha}+\frac{p\chi}{s+2\alpha}\right)Y_0, \tag{5.6}$$

where we have used (4.13) and (5.2). Thus, we quote the solution only for Y_0:

$$Y_0 = -\frac{1}{3(s+\alpha)}\left[2+\frac{pA_0}{60(s+\lambda)}\right], \quad \lambda = \alpha + pA_0b, \quad b = \delta_y^2 - \frac{1}{6}. \tag{5.7}$$

Substituting (5.7) into (5.6) and inverting the Laplace transform, we have

$$\langle B_y\rangle = \frac{D\chi}{6\alpha}\left\{\left(2+\frac{1}{60b}\right)\left[\frac{(\mathrm{e}^{-\alpha t}-1)p\chi}{\alpha} - Kt\right]\mathrm{e}^{-\alpha t} + \frac{K(\mathrm{e}^{-\alpha t}-\mathrm{e}^{-\lambda t})}{60pA_0b^2} + \frac{p\chi(\mathrm{e}^{-2\alpha t}-\mathrm{e}^{-\lambda t})}{60b(\lambda-2\alpha)}\right\}. \tag{5.8}$$

Then, averaging (4.11) and substituting the result along with (5.8) into the average of (4.10), we obtain

$$\begin{aligned}\bar{B}_1(t) = &\frac{\chi\mathrm{e}^{-\alpha t}}{\alpha}\left[\frac{(\mathrm{e}^{-\alpha t}-1)p\chi}{\alpha} - Kt\right]\left[\bar{h}+\frac{D}{6}\left(2+\frac{1}{60b}\right)\right]\\ &+\frac{D\chi}{360\alpha b}\left[\frac{K(\mathrm{e}^{-\alpha t}-\mathrm{e}^{-\lambda t})}{pA_0b} + \frac{p\chi(\mathrm{e}^{-2\alpha t}-\mathrm{e}^{-\lambda t})}{(\lambda-2\alpha)}\right],\end{aligned} \tag{5.9a}$$

$$\bar{h} = \frac{3^{5/3}(x_{\max}^{4/3}-x_{\min}^{4/3})}{4\Gamma(2/3)(x_{\max}-x_{\min})}. \tag{5.9b}$$

5.2 *Results*

As before, we examine the limit that $\delta_y \to \infty$ to verify our results against previous work. In this limit, we see from (5.7), (5.1) and (5.4) that

$$b \sim \delta_y^2, \quad r \sim 2\delta_y, \quad A_0 \sim -\frac{1}{\delta_y^2}, \quad \lambda \sim K.$$

Substituting these results into (5.9a), we have

$$\bar{B}_1(t) = \left[\frac{(\mathrm{e}^{-\alpha t} - 1)p\chi}{\alpha} - Kt\right]\frac{\chi\,\mathrm{e}^{-\alpha t}}{\alpha}\bar{h}_\mathrm{g}, \quad \bar{h}_\mathrm{g} = \left(\bar{h} + \frac{D}{3}\right). \tag{5.10}$$

Note that if we replace p by 1, (5.10) becomes the result from the receptor layer case without any blocking (Edwards, 2001). Physically, this says that in the limit of very large d_l, the occlusion effects due to the ligand's large size swamp any effect they may have in the thin receptor layer.

Taking the limit $H_\mathrm{g} \to 0$ to reduce to the 2D case with blocking means that $D \to 0$ as well, in which case (5.10) becomes

$$\bar{B}_1(t) = \left[\frac{(\mathrm{e}^{-\alpha t} - 1)p\chi}{\alpha} - Kt\right]\frac{\chi\,\mathrm{e}^{-\alpha t}}{\alpha}\bar{h}, \tag{5.11}$$

which is exactly the result in Edwards (2007).

Figure 9 shows the effect of changing d_l on $\bar{B}_0$ as given in (4.7) with the parameters in Table 1. Note that we have chosen to fix the value of H_g at a (high) level, so changing δ_y and p is accomplished by changing d_l. Note that with no hindrance effects ($p = 1$) and the value of K given, the steady state of $\bar{B}_0$ would be 1/2. Since the fact that $d_\mathrm{l} \geqslant H_\mathrm{g}$ immediately implies that $d_\mathrm{l} \geqslant d_\mathrm{r}$, we are in the case with high p and large occlusion effects. As expected, increasing d_l lowers the steady-state value and decreases the timescale needed to achieve the maximum value.

Figure 10 shows the effect of changing d_l on $\bar{B}_1$ as given in (5.9a). Here, the increasing d_l values increase b, which causes an algebraic decay in the solution. At first blush, it may seem that these are

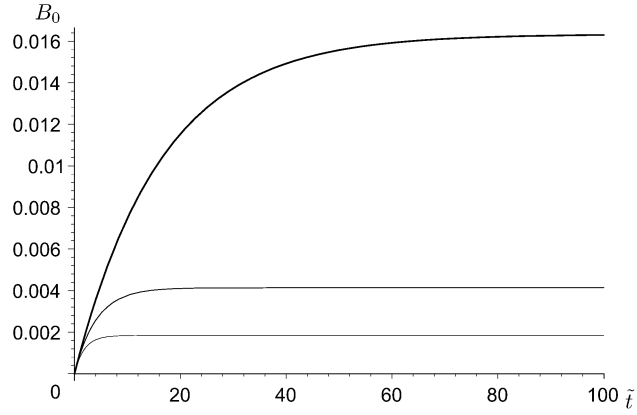

FIG. 9. $\bar{B}_0$ versus $\tilde{t}$ with $K = 1$ and (in decreasing order of thickness) $d_\mathrm{l} = H_\mathrm{g}, 2H_\mathrm{g}, 3H_\mathrm{g}$.

TABLE 1 *Parameter values for Figs 9–12*

Given		Calculated	
Parameter	Value	Parameter	Value
B_i	0	t	$10^{-3}\,\tilde{t}$/s
C_u (mol/cm^3)	10^{-11}	χ	1
D	1.20×10^{-1}		
Da	10^{-1}		
H_g (cm)	10^{-5}		
$\tilde{k}_\mathrm{a}$ (cm^3/mol/s)	10^{8}		
R_T (mol/cm^2)	10^{-12}		
x_max	7.92×10^{-1}		
x_min	2.08×10^{-1}		

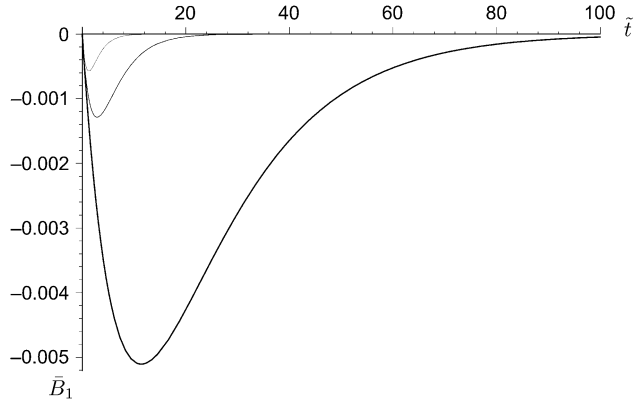

FIG. 10. $\bar{B}_1$ versus $\tilde{t}$ with $K = 1$ and (in decreasing order of thickness) $d_\mathrm{l} = H_\mathrm{g}, 2H_\mathrm{g}, 3H_\mathrm{g}$.

large effects since the size of $\bar{B}_1$ and $\bar{B}_0$ is similar. However, since $\bar{B}_1$ must be multiplied by Da (assumed small) before contributing to the solution, the relative contribution is O(Da).

We conclude with a note about the effective rate constant (ERC) formulation, which usually can reduce the small-Da case to an ordinary differential equation for the sensogram signal $\bar{B}_\mathrm{g}$ (Edwards *et al.*, 1999). This is customarily done by manipulating (2.6) into the form

$$\frac{\partial B_\mathrm{g}}{\partial t} - \mathrm{Da}(1 - pB_0)\frac{\mathrm{d}B_0}{\mathrm{d}t}\left\{D\left[\frac{y(y+2)}{2}\right] - h(x)\right\} = 1 - \mathcal{S}[B_\mathrm{g}] - KB_\mathrm{g} + \mathrm{O}(\mathrm{Da}^2) \tag{5.12}$$

and then averaging. But in this instance, averaging yields a term of the form $\overline{\mathcal{S}[B_\mathrm{g}]}$, which cannot be expressed in terms of $\mathcal{S}[\bar{B}_\mathrm{g}]$. Hence, this approach fails for the association experiment. Nevertheless, it will be shown to be effective for a dissociation experiment in Section 6.

6. Dissociation experiment

A typical run of the BIAcore includes both an association phase and a dissociation phase that begins when the association experiment reaches steady state. From (3.5), we see that as $t \to \infty$, $F_y \to 0$, so

from (3.7) we have that $F_x \to 0$ and hence $C_g \to 0$. Then, using the same arguments in Section 3, we find that the steady state of (3.9) is

$$B_{g,s} = \frac{1}{\alpha}, \tag{6.1}$$

which provides the initial condition for the dissociation problem. In addition, the ligand concentration is shut off, so the equation analogous to (3.9) is

$$\frac{\partial B_g}{\partial t} = \{1 - \mathcal{S}[B_g]\}\mathrm{Da}(DF_y + F_x) - KB_g. \tag{6.2}$$

The fact that the integral term first appears at O(Da) is critical to explaining the simplifications that follow.

Substituting (4.1) into (6.1) and (6.2), we have

$$\frac{\partial B_0}{\partial t} = -KB_0, \quad B_0(x, y, 0) = \alpha^{-1}, \tag{6.3a}$$

$$\frac{\partial B_1}{\partial t} = \{1 - \mathcal{S}[B_0]\}(DF_y + F_x) - KB_1, \quad B_1(x, y, 0) = 0. \tag{6.3b}$$

Solving (6.3a), we obtain

$$B_0(x, y, t) = \bar{B}_0(t) = \frac{\mathrm{e}^{-Kt}}{\alpha}. \tag{6.4}$$

Equations (4.8) do not change since all the changes are incorporated into the new value of $\mathrm{d}B_0/\mathrm{d}t$.

Since B_0 is independent of x and y, we see from (2.15) that (6.3b) becomes

$$\frac{\partial B_1}{\partial t} + KB_1 = -\left(1 - p\frac{\mathrm{e}^{-Kt}}{\alpha}\right)\left(-\frac{K\,\mathrm{e}^{-Kt}}{\alpha}\right)\left\{D\left[\frac{y(y+2)}{2}\right] - h(x)\right\}, \tag{6.5}$$

where we have used (4.8) and (6.4). Thus, the integral term does not appear to first two orders and the only difference between this result and the 2D occlusion result in Edwards (2007) is the replacement of $-h(x)$ by the braced term. Solving (6.5) subject to the initial condition in (6.3b), we obtain

$$B_1 = -\frac{K}{\alpha}\left[t + \frac{p(\mathrm{e}^{-Kt} - 1)}{K\alpha}\right]\mathrm{e}^{-Kt}\left\{D\left[\frac{y(y+2)}{2}\right] - h(x)\right\}. \tag{6.6}$$

Averaging then yields

$$\bar{B}_1(t) = \frac{K\,\mathrm{e}^{-Kt}}{\alpha}\left[t + \frac{p(\mathrm{e}^{-Kt} - 1)}{K\alpha}\right]\bar{h}_g. \tag{6.7}$$

To proceed with an ERC formulation, we note that the equation analogous to (5.12) is

$$\frac{\partial B_g}{\partial t} - \mathrm{Da}(1 - pB_0)\frac{\mathrm{d}B_0}{\mathrm{d}t}\left\{D\left[\frac{y(y+2)}{2}\right] - h(x)\right\} = -KB_g + \mathrm{O}(\mathrm{Da}^2). \tag{6.8}$$

With the $\mathcal{S}[B_g]$ term now relegated to lower order, we can take the average of (6.8) to obtain

$$\frac{d\bar{B}_g}{dt} = -\frac{K\bar{B}_g}{1 + \mathrm{Da}(1 - p\bar{B}_g)\bar{h}_g} + \mathrm{O}(\mathrm{Da}^2), \tag{6.9}$$

which (with the exception of the p term) is exactly the result from the receptor layer work without occlusion (Edwards, 2001).

Figure 11 shows the effect of p on the dissociation solution. Note that the only difference from the result in Edwards (2007) for 2D occlusion effects is the introduction of the extra $D/3$ term, which is quite small from Table 1. Thus, our plots are quite similar to those in Edwards (2007), except that p in our work now plays the role of p^2 in Edwards (2007). In particular, increasing p reduces the binding.

Figure 12 shows the same graph for $K = 10$. Note that though on a relative basis the effect of p is about the same, on an absolute basis it is not since K dominates the α portion of the denominator of the steady state. Again, the work is quite similar to the 2D work.

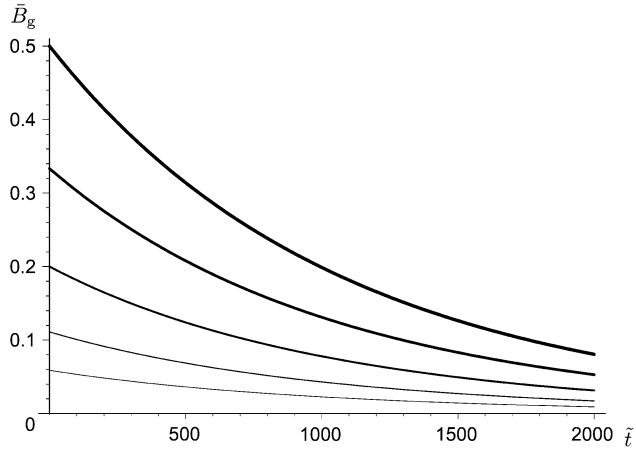

FIG. 11. $\bar{B}_g$ versus $\tilde{t}$ with $K = 1$ and (in decreasing order of thickness) $p = 1, 2, 4, 8, 16$.

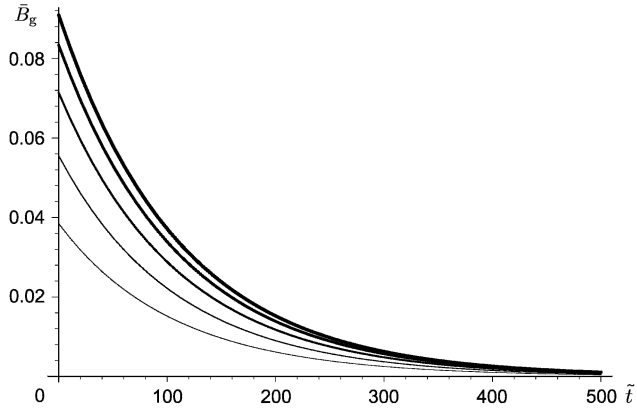

FIG. 12. $\bar{B}_g$ versus $\tilde{t}$ with $K = 10$ and (in decreasing order of thickness) $p = 1, 2, 4, 8, 16$.

7. Moderate Da

7.1 *Association experiment*

Though it is desirable from an experimental standpoint to make Da small, in some situations (such as in very fast reactions) such a state is unattainable. Thus, we now present results in the case where Da is moderate. In this case, (3.9) is non-linear. To linearize the problem, we resort to small-time asymptotics by assuming a solution of the form

$$B_{\mathrm{g}}(x,y,t) = B_{\mathrm{i}} + \beta(x,y)t + \mathrm{o}(t). \tag{7.1}$$

With such a substitution, we define a new variable F_1 in the following manner:

$$\frac{\partial^2 F_1}{\partial y^2} = \beta, \quad \frac{\partial F_1}{\partial y}(x,-1) = 0, \quad F_1(x,0) = 0. \tag{7.2}$$

Then, substituting (7.1) and (7.2) into (2.6), we obtain, to leading order in t,

$$1 - pB_{\mathrm{i}} - (\beta + KB_{\mathrm{i}}) = \mathrm{Da}(1-pB_{\mathrm{i}})\left[\frac{1}{3^{1/3}\Gamma(2/3)}\int_0^x \frac{\partial F_1}{\partial y_{\mathrm{d}}}(x-\xi,0)\frac{\mathrm{d}\xi}{\xi^{2/3}} - DF_1\right]. \tag{7.3}$$

Note in particular that the integral term does not come into play since the leading order is assumed to be constant. Thus, our work will be quite similar to previous results in Edwards (2001, 2007).

Since the sensogram signal is averaged, we are more interested in the quantity

$$\langle\beta\rangle = \frac{\partial F_1}{\partial y}(x,0), \tag{7.4}$$

where we have used (7.2). Thus, it is easiest to work directly with F_1 in (7.3), which we solve with the use of Laplace transforms (in x, rather than t):

$$\frac{\mathrm{d}^2\hat{F}_1}{\mathrm{d}y^2} - \lambda_{\mathrm{a}}^2\hat{F}_1 = \frac{\chi}{s} - \frac{\nu^{1/3}}{s^{1/3}}\frac{\mathrm{d}\hat{F}_1}{\mathrm{d}y}(0), \tag{7.5a}$$

$$\nu = \frac{1}{3}\left[\frac{\mathrm{Da}(1-pB_{\mathrm{i}})\Gamma(1/3)}{\Gamma(2/3)}\right]^3, \quad \lambda_{\mathrm{a}}^2 = D\mathrm{Da}(1-pB_{\mathrm{i}}), \tag{7.5b}$$

which is exactly the equation from Edwards (2001) with a different definition of ν and λ_{a} to include the occlusion contribution through the parameter p.

Then, we may write the average as

$$\bar{B}_{\mathrm{g}}(t) = B_{\mathrm{i}} + S\tilde{t} + \mathrm{o}(t), \quad S = \frac{\tilde{k}_{\mathrm{a}}C_{\mathrm{u}}\{\mathcal{I}[\beta;x_{\max}] - \mathcal{I}[\beta;x_{\min}]\}}{x_{\max}-x_{\min}}, \tag{7.6}$$

$$\mathcal{I}[\beta;x] = \frac{\chi\,\mathrm{e}^{-\nu_{\mathrm{a}}x}}{\nu_{\mathrm{a}}}\frac{\tanh\lambda_{\mathrm{a}}}{\lambda_{\mathrm{a}}}[\mathrm{e}^{\nu_{\mathrm{a}}x} - 1 - |P(4/3,-\nu_{\mathrm{a}}x)| + |P(5/3,-\nu_{\mathrm{a}}x)|], \tag{7.7a}$$

$$\nu_{\mathrm{a}} = \frac{\nu\tanh^3\lambda_{\mathrm{a}}}{\lambda_{\mathrm{a}}^3}. \tag{7.7b}$$

Here, $\mathcal{I}$ is simply the integral of $\langle\beta\rangle$:

$$\mathcal{I}[\beta; x] \equiv \int_0^x \langle\beta\rangle \mathrm{d}\xi \tag{7.8a}$$

and P is the normalized *lower* incomplete gamma function whose definition is

$$P(m/3, -\nu_\mathrm{a} x) = \frac{\gamma\,(m/3, -\nu_\mathrm{a} x)}{\Gamma(m/3)}. \tag{7.8b}$$

We next examine the asymptotic limits of (7.7a), relying heavily on the analysis in Edwards (2001). In the limit of small $\tilde{k}_\mathrm{a}$, the functional dependence of $\mathcal{I}$ on ν_a and λ_a vanishes, as the limits are independent of those quantities. In particular,

$$\mathcal{I}[\beta; x] \sim \chi x \Longrightarrow S \sim \tilde{k}_\mathrm{a} C_\mathrm{u}[1 - (K + p)B_\mathrm{i}] \quad \text{as } \tilde{k}_\mathrm{a} \to 0. \tag{7.9}$$

We do not expand the bracketed quantity because we are treating K as fixed. In typical experiments (which we shall graph below), $B_\mathrm{i} = 0$, so both dissociation and occlusion effects are absent. However, in the case where $B_\mathrm{i} \neq 0$, we see that both dissociation (through the K term) and occlusion effects (through the p term) will slow the initial rate of growth of the sensogram data.

Examining the asymptote for large $\tilde{k}_\mathrm{a}$, we see that

$$\mathcal{I}[\beta; x] \sim \frac{\chi x^{2/3}}{\nu^{1/3}\Gamma(5/3)}, \tag{7.10}$$

and hence there is a finite asymptote for S. This is due to the fact that the reaction rate becomes infinitely fast, so the system becomes transport limited. Here,

$$\lim_{\tilde{k}_\mathrm{a} \to \infty} \chi = 1 - pB_\mathrm{i}, \tag{7.11}$$

so we see that occlusion effects will tend to slow the initial rate of growth of the sensogram data at a rate proportional to the initial number of receptors bound.

In the experiments that we are modelling, $B_\mathrm{i} = 0$, so the dependence on p in (7.10) cancels and we are left with the result from Edwards (2007):

$$S \sim \frac{3^{4/3} C_\mathrm{u} V^{1/3} \tilde{D}_\mathrm{f}^{2/3} (x_\mathrm{max}^{2/3} - x_\mathrm{min}^{2/3})}{2\Gamma(1/3) R_\mathrm{T} L^{1/3} H_\mathrm{f}^{1/3} (x_\mathrm{max} - x_\mathrm{min})}, \quad \tilde{k}_\mathrm{a} \to \infty. \tag{7.12}$$

Since the reaction is infinitely fast, the effect of D is negligible, and hence the two results are identical. Thus, there is some maximal rate due to transport, and the mode of transport is unimportant.

Figure 13 shows how the slope S varies with $\tilde{k}_\mathrm{a}$ using the parameters in Table 2. Note that p appears only when multiplied by B_i (directly or through α). Since $B_\mathrm{i} = 0$, p does not affect our results. Physically, this means that for small times, there has not been enough binding for occlusion effects to play a role. For the parameters in Table 2, the asymptote in Fig. 13 may be calculated as

$$S = 2.81 \times 10^{-3}\ \mathrm{s}^{-1}, \quad \tilde{k}_\mathrm{a} \to \infty. \tag{7.13}$$

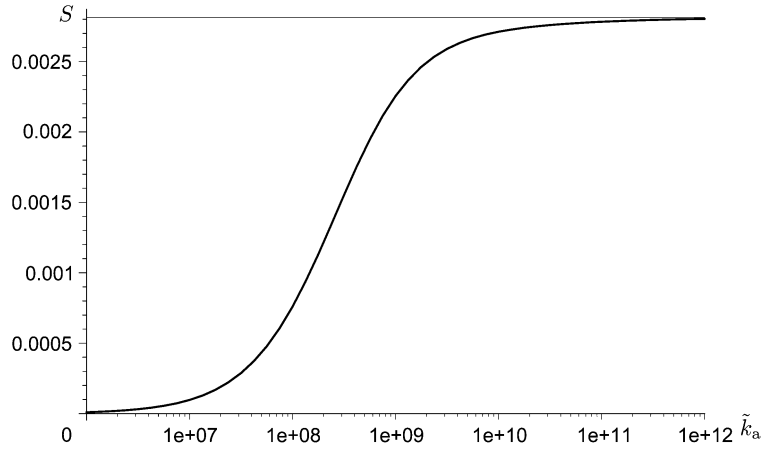

FIG. 13. S versus $\tilde{k}_a$, association experiment.

TABLE 2 *Parameter values for Figs* 13–15

Given		Calculated	
Parameter	Value	Parameter	Value
B_i	0	χ	1
C_u (mol/cm^3)	10^{-11}		
$\tilde{D}_f$ (cm^2/s)	2.8×10^{-7}		
D	1.20×10^{-1}		
H_f (cm)	5×10^{-3}		
L (cm)	2.4×10^{-1}		
R_T (mol/cm^2)	10^{-12}		
V (cm/s)	1		
x_{max}	7.92×10^{-1}		
x_{min}	2.08×10^{-1}		

7.2 *Dissociation experiment*

Lastly, we examine the dissociation case. As discussed previously, the initial condition here is the steady state from the association problem, given in (6.1). Thus, the equation analogous to (7.5a) is

$$\frac{\mathrm{d}^2\hat{F}_1}{\mathrm{d}y^2} - \lambda_\mathrm{d}^2\hat{F}_1 = -\frac{K}{\alpha s} - \frac{\mu^{1/3}}{s^{1/3}}\frac{\mathrm{d}\hat{F}_1}{\mathrm{d}y}(0), \tag{7.14a}$$

$$\mu = \frac{1}{3}\left[\frac{\mathrm{Da}K\Gamma(1/3)}{\alpha\Gamma(2/3)}\right]^3, \quad \lambda_\mathrm{d}^2 = \frac{D\mathrm{Da}K}{\alpha}. \tag{7.14b}$$

Since (7.14a) is the same as (7.5a) except for the replacement of χ by $-K/\alpha$, (7.7a) becomes

$$\mathcal{I}[\beta_1; x] = -\frac{K\,\mathrm{e}^{-\nu_\mathrm{d}x}}{\alpha\nu_\mathrm{d}}\frac{\tanh\lambda_\mathrm{d}}{\lambda_\mathrm{d}}[\mathrm{e}^{\nu_\mathrm{d}x} - 1 - |P(4/3, -\nu_\mathrm{d}x)| + |P(5/3, -\nu_\mathrm{d}x)|], \tag{7.15a}$$

$$\nu_{\mathrm{d}} = \frac{\mu \tanh^3 \lambda_{\mathrm{d}}}{\lambda_{\mathrm{d}}^3}. \tag{7.15b}$$

Since $\mathrm{Da} \to 0$ as $\tilde{k}_{\mathrm{a}} \to 0$, in this limit $\nu_{\mathrm{d}} \to 0$ and $\lambda_{\mathrm{d}} \to 0$, so we may use the expression in (7.9), simply replacing χ by $-K/\alpha$. But with $\tilde{k}_{\mathrm{d}}$ fixed, $\tilde{k}_{\mathrm{a}} \to 0$ forces this ratio to be -1. Thus, we have

$$S \sim -\tilde{k}_{\mathrm{a}} C_{\mathrm{u}}, \quad \tilde{k}_{\mathrm{a}} \to 0, \quad \tilde{k}_{\mathrm{d}} \text{ fixed}, \tag{7.16}$$

which is independent of p. Physically, since blocking is related to the association process, a small $\tilde{k}_{\mathrm{a}}$ implies that blocking will not have time to develop for small t.

In the case of large $\tilde{k}_{\mathrm{a}}$, it can be shown that

$$\lim_{\tilde{k}_{\mathrm{a}} \to \infty} \lambda_{\mathrm{d}} = \lambda_\infty = \left(\frac{\tilde{R}_{\mathrm{T}} H_{\mathrm{g}}}{\phi \tilde{D}_{\mathrm{g}}} \frac{\tilde{k}_{\mathrm{d}}}{p C_{\mathrm{u}}} \right)^{1/2}, \tag{7.17a}$$

$$\lim_{\tilde{k}_{\mathrm{a}} \to \infty} \nu_{\mathrm{d}} = \nu_\infty = \frac{1}{3\mathrm{Pe}_{\mathrm{f}}} \left[\frac{\Gamma(1/3)}{\Gamma(2/3)} \frac{\tilde{R}_{\mathrm{T}} H_{\mathrm{f}}}{\tilde{D}_{\mathrm{f}}} \frac{\tilde{k}_{\mathrm{d}}}{p C_{\mathrm{u}}} \frac{\tanh \lambda_\infty}{\lambda_\infty} \right]^3. \tag{7.17b}$$

Since ν_∞ decays like p^{-3}, we may use the small-argument asymptotic expansion for the P function to obtain

$$\mathcal{I}[\beta_1; x] \sim -\frac{\tilde{k}_{\mathrm{d}} x}{p \tilde{k}_{\mathrm{a}} C_{\mathrm{u}}}, \tag{7.18}$$

and hence larger values of p will drive down the value of the asymptote.

As in previous sections, we will examine graphically how the dependence of the solution on $\tilde{k}_{\mathrm{a}}$ varies with p. Thus, we must fix a value of $\tilde{k}_{\mathrm{d}}$ (instead of K, as in Section 7.1).

Figure 14 shows the graph of $|S|$ versus $\tilde{k}_{\mathrm{a}}$ with $\tilde{k}_{\mathrm{d}} = 8.9 \times 10^{-3}\ \mathrm{s}^{-1}$ and varying p. We have graphed $-S$ so that easy comparisons can be made with the association diagram. Note that increasing

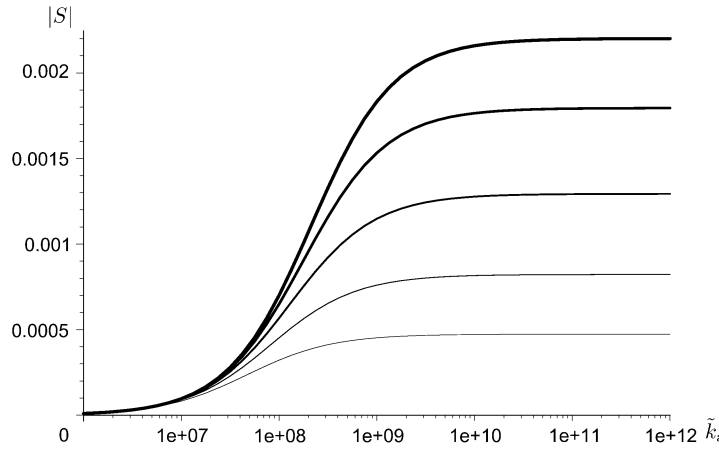

FIG. 14. $|S|$ versus $\tilde{k}_{\mathrm{a}}$ with $\tilde{k}_{\mathrm{d}} = 8.9 \times 10^{-3}\ \mathrm{s}^{-1}$ and (in decreasing order of thickness) $p = 1, 2, 4, 8, 16$.

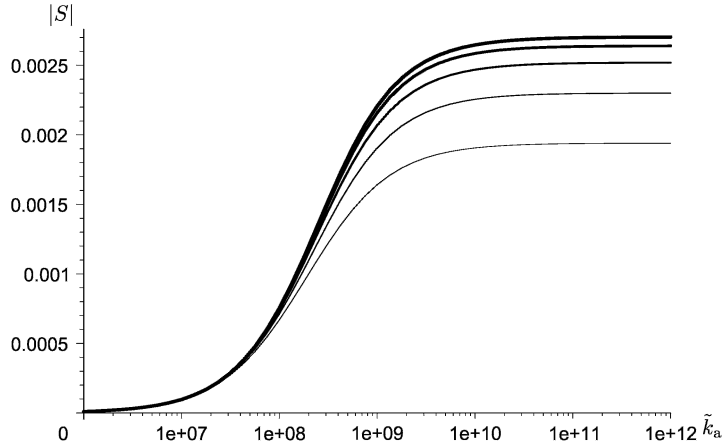

FIG. 15. $|S|$ versus $\tilde{k}_a$ with $\tilde{k}_d = 8.9 \times 10^{-2}$ s^{-1} and (in decreasing order of thickness) $p = 1, 2, 4, 8, 16$.

p reduces the initial speed of dissociation, with the most dramatic trends being shown as $\tilde{k}_a$ gets large. This makes sense since with larger $\tilde{k}_a$, the inherent timescale of the problem decreases.

In Fig. 12, we increased K by a factor of 10 to illustrate the effect of p in a different circumstance. To achieve the same result in this context, we increase $\tilde{k}_d$ by a factor of 10, as shown in Fig. 15. Note that just as in Section 4, the effects of p are mitigated with increasing $\tilde{k}_d$. This is because dissociation plays a larger role in the reaction, and dissociation is unaffected by steric hindrance.

8. Conclusions

To better analyse and control biological and industrial processes, the underlying kinetic processes must be well understood. Since the BIAcore SPR device consists of a thin reacting zone abutting a larger fluid flow, it is a good physical model of many biological and industrial reactions. However, the real-time kinetic data thus obtained are useless for parameter estimation without a proper mathematical model to interpret it.

In particular, when the ligand molecules are larger than the spacing of the receptor molecules in the zone, a single binding event will occlude multiple binding sites. Without taking this steric hindrance effect into account, one will obtain inaccurate estimates of the underlying rate constants. We presented some general discussion of the modelling process in Section 2.1. In order to obtain a tractable set of equations, we made several simplifying assumptions about the position and behaviour of the binding site. However, we expect these assumptions to be unbiased, so the averaging properties of the BIAcore signal should reduce any associated errors.

Mathematically, we model the occlusion event as a non-local integral term in the evolution equation for B_g. As in Edwards (2007), the small size of the ligand molecules compared to the channel length meant that the non-locality in the x-direction can be neglected. However, the ligand molecule can be comparable in size to the width of the receptor layer, and hence the integral term in the y-direction must be treated fully.

We specialized to the case of large molecules so that the integral term assumed a separable Fredholm form. (The case of smaller molecules is the object of further research.) Scientists prefer to work in the regime where Da is small to limit the effects of transport; in this case, we constructed solutions good for

long times which were accurate to $O(Da^2)$. The integral term arose only in the association experiment since in that case the integral term is non-trivial at the first two orders. Since the average of the integral term cannot be expressed in terms of $\bar{B}_g$, we could obtain an ERC solution only in the dissociation case.

In the case of moderate Da, we constructed analytical short-time solutions. Due to the nature of the dominant balance, the integral term does not contribute. Hence, our results can be interpreted as a blend of the receptor layer work without occlusion in Edwards (2001) and the surface reaction work in Edwards (2007).

In the cases without the integral term, the steric hindrance effect is encapsulated in the parameter p, which measures the ratio of the occluded areas of ligand to receptor. Though the effect can most easily be seen in (4.6), the parameter p propagates throughout the solutions. The dependence of p on d_l is quadratic while the dependence on R_T is linear, and hence d_l is the dominant factor in determining whether or not blocking will occur.

Since R_T must be kept at a relatively high level to distinguish the BIAcore signal from experimental noise, it is clear from the Appendix that there will be cases where steric hindrance effects are unavoidable. To minimize them, experimentalists can reduce R_T as much as possible to reduce p and thus the *absolute* steric hindrance effect. The *relative* size of the steric hindrance effect may be reduced by increasing K, as seen in (4.6). From (2.6), we see that this may be affected by decreasing C_u.

9. Nomenclature

9.1 *Variables and parameters*

Units are listed in terms of length (L), mass (M), moles (N) or time (T). If the same letter appears both with and without tildes, the letter with a tilde has dimensions, while the letter without a tilde is dimensionless. The equation where a quantity first appears is listed, if appropriate.

$A(y)$: function used to characterize $\mathcal{S}_0$ (5.1).

$\tilde{B}(\tilde{x}, \tilde{y}, \tilde{t})$: bound ligand concentration at position $(\tilde{x}, \tilde{y}, \tilde{t})$ and time $\tilde{t}$, units N/L^2.

b: dimensionless parameter (5.7).

$\tilde{C}(\tilde{x}, \tilde{y}, \tilde{t})$: unbound ligand concentration at position $(\tilde{x}, \tilde{y})$ and time $\tilde{t}$, units N/L^3 (2.1).

$\mathcal{C}$: the Bromwich contour.

$\tilde{D}$: molecular diffusion coefficient, units L^2/T (2.5a).

d: spacing between molecules, units L.

Da: the Damköhler number, which measures the ratio of reaction and diffusion effects, dimensionless (2.5a).

$F(\cdot, t)$: function used to characterize C_g (3.5).

$f(\cdot)$: arbitrary function, variously defined.

H: height, units L.

$h(x)$: function used in ERC solution (4.8b).

$\mathcal{I}[\beta; x]$: integration operator, defined in (7.8a) as

$$\mathcal{I}[\beta; x] \equiv \int_0^x \langle\beta\rangle \mathrm{d}\xi.$$

K: dimensionless affinity constant (2.6).

$\tilde{k}_d$: dissociation rate, units T^{-1} (2.1).

$\tilde{k}_a$: association rate, units $L^3/(NT)$.
L: length of the channel, units L (2.1).
m: arbitrary integer, variously defined.
N: Avogadro's number, units N^{-1} (2.13).
$P(\cdot,\cdot)$: normalized lower incomplete gamma function (7.8b).
p: volume ratio of ligand to receptor molecule (2.12).
Pe: Peclét number for the system (2.5b).
R_T: density of receptor sites, units N/L^2 (2.1).
r: dimensionless parameter (5.1).
$\tilde{\mathcal{S}}[\cdot]$: steric hindrance operator (2.1).
S: slope of sensogram data for small time, units T^{-1} (7.6).
s: Laplace transform variable.
$\tilde{t}$: time, units T (2.1).
V: characteristic flow velocity, units L/T (2.5b).
$\tilde{x}$: length along the channel, units L.
$Y(y)$: intermediate variable related to $\hat{B}_y$ (4.13).
$\tilde{y}$: height above reacting surface, units L (2.1).
$\mathcal{Z}$: the integers.
$\tilde{z}$: distance perpendicular to flow, units L.
α: dimensionless constant, defined as $K + p$ (4.2a).
$\beta(x)$: term in expansion of $B(x,t)$ for small t (7.1).
δ: ratio of ligand radius to characteristic length (2.9a).
λ: dimensionless parameter, variously defined.
μ: dimensionless parameter in moderate Da case (7.14b).
ν: dimensionless parameter in moderate Da case (7.5b).
ξ: dummy variable, variously defined.
χ: dimensionless constant, value $1 - \alpha B_i$ (4.11).
ϕ: partition coefficient (2.1).

9.2 *Other notations*

a: as a subscript, used to indicate association.
d: as a subscript, used to indicate dissociation.
f: as a subscript, used to indicate the flow (2.5a).
g: as a subscript, used to indicate the dextran gel layer.
i: as a subscript, used to indicate an initial condition (3.1).
l: as a subscript, used to indicate the ligand.
$m \in \mathcal{Z}$: as a subscript, used to indicate a normalization factor (2.2), an expansion (4.1) or integration against a test function (5.2).
max: as a subscript on x, used to indicate the right end point of the scanning range (3.2); as a subscript on y or ξ, used to indicate an upper limit of integration (2.3b).

min: as a subscript on x, used to indicate the left end point of the scanning range (3.2); as a subscript on y or ξ, used to indicate an upper limit of integration (2.3b).

r: as a subscript, used to indicate the receptor.

s: as a subscript, used to indicate the steady state (2.10).

u: as a subscript on C, used to indicate a characteristic value (2.4a).

x: as a subscript, used to indicate the x-direction (2.9a).

y: as a subscript, used to indicate the y-direction (2.9a).

(2): as a superscript, refers to the 2D analog of this problem, described in Edwards (2007) (2.19b).

*: as a subscript, refers to a constant value.

$\bar{\ }$: used to denote the BIAcore signal, which is the mean of the bound concentration (3.2).

$\hat{\ }$: used to denote the Laplace transform of a quantity.

∞: as a subscript, refers to a limiting value as $\tilde{k}_a \to \infty$ (7.17a).

$\langle\ \rangle$: used to indicate the average in the y-direction only (3.2).

$'$: used to indicate a dummy variable (2.2).

Appendix

We conclude with a brief discussion of the dimensionless parameters used in this work. Table A1 summarizes some extreme values of the parameters found in the literature, which we use to establish bounds on our dimensionless parameters. Note that d_l is a *diameter*, while most papers quote the Stokes *radius*.

To compute a lower bound for δ_y, we use the lower bound on d_l from Curto *et al.* (2005) and the upper bound on H_g from Edwards *et al.* (1995). Similarly, to compute an upper bound for δ_y, we use the upper bound on d_l from Zheng & Rundell (2003) and the lower bound on H_g from Schuck (1996). The computed range is

$$8 \times 10^{-3} \leqslant \delta_y \leqslant 50. \tag{A.1}$$

Therefore, both the $\delta_y < 1$ and the $\delta_y > 1$ cases are physically realizable.

For the attainable values of p, one can trivially attain the lower bound of 1 with very small ligand molecules or wide receptor spacing. For the upper bound, we note that (2.13) becomes

$$p = d_l^2 N R_T \tag{A.2}$$

TABLE A1 *Parameter values from the literature*

	Parameter		
Reference	d_l (10^{-6} cm)	H_g (10^{-5} cm)	R_T (10^{-12} mol/cm^2)
Curto *et al.* (2005)	0.4		
Edwards *et al.* (1995)		2–5	
Schuck (1996)		0.1–1	
Yarmush *et al.* (1996)			0.25–4
Zheng & Rundell (2003)	50		0.065

for large d_1, which is exactly the expression for p^2 in Edwards (2007). Thus, we may quote the upper bound from that work to construct the possible range of p:

$$1 \leqslant p \leqslant 6.02 \times 10^3. \tag{A.3}$$

Funding

National Institute of General Medical Sciences (1R01GM067244-01).

Acknowledgements

The author thanks the reviewer for his thoughtful and insightful comments; they greatly improved the manuscript. Many of the calculations herein were checked with the assistance of Maple.

References

Curto, L. M., Caramelo, J. J. & Delfino, J. M. (2005) Δ98Δ, a functional all-β-sheet abridged form of intestinal fatty acid binding protein. *Biochemistry*, **44**, 13847–13857.

Edwards, D. A. (2001) The effect of a receptor layer on the measurement of rate constants. *Bull. Math. Biol.*, **63**, 301–327.

Edwards, D. A. (2007) Steric hindrance effects on surface reactions: applications to BIAcore. *J. Math. Biol.*, **55**, 517–539.

Edwards, D. A., Goldstein, B. & Cohen, D. S. (1999) Transport effects on surface-volume biological reactions. *J. Math. Biol.*, **39**, 533–561.

Edwards, P. R., Gill, A., Pollardknight, D. V., Hoare, M., Buckle, P. E., Lowe, P. A. & Leatherbarrow, R. J. (1995) Kinetics of protein-protein interactions at the surface of an optical biosensor. *Anal. Biochem.*, **231**, 210–217.

Garland, P. B. (1996) Optical evanescent wave methods for the study of biomolecular reactions. *Q. Rev. Biophys.*, **29**, 91–117.

Gherardi, E., Youles, M. E., Miguel, R. N., Blundell, T. L., Iamele, L., Gough, J., Bandyopadhyay, A., Hartmann, G. & Butler, P. J. G. (2003) Functional map and domain structure of MET, the product of the c-met protooncogene and receptor for hepatocyte growth factor scatter factor. *Proc. Natl. Acad. Sci.*, **100**, 12039–12044.

Goldstein, B. & Dembo, M. (1995) Approximating the effects of diffusion on reversible reactions at the cell surface: ligand-receptor kinetics. *Biophys. J.*, **68**, 1222–1230.

Grabowski, E. F., Friedman, L. I. & Leonard, E. F. (1972) Effects of shear rate on the diffusion and adhesion of blood platelets to a foreign surface. *Ind. Eng. Chem. Fundam.*, **11**, 224–232.

Jansen, J. & Niemeyer, B. (2005) Automated high-pressure plant for a continuous flow through a fixed bed investigation of hydrodynamic behaviour. *J. Supercrit. Fluids*, **33**, 283–291.

Karlsson, R. & Fält, A. (1997) Experimental design for kinetic analysis of protein-protein interactions with surface plasmon resonance biosensors. *J. Immunol. Methods*, **200**, 121–133.

Karlsson, R., Michaelson, A. & Mattson, L. (1991) Kinetic analysis of monoclonal antibody-antigen interactions with a new biosensor based analytical system. *J. Immunol. Methods*, **145**, 229–240.

Liedberg, B., Lundstrom, I. & Stenberg, E. (1993) Principles of biosensing with an extended coupling matrix and surface-plasmon resonance. *Sens. Actuators B*, **11**, 63–72.

Long, W. M. & Kalachev, L. V. (2000) Asymptotic analysis of dissolution of a spherical bubble (case of fast reaction outside the bubble). *Rocky Mt. J. Math.*, **30**, 293–313.

Mann, S., Burkett, S. L., Davis, S. A., Fowler, C. E., Mendelson, N. H., Sims, S. D., Walsh, D. & Whilton, N. T. (1997) Sol-gel synthesis of organized matter. *Chem. Mater.*, **9**, 2300–2310.

RAGHAVAN, M., CHEN, M. Y., GASTINEL, L. N. & BJORKMAN, P. J. (1994) Investigation of the interaction between the class I MHC-related Fc receptor and its immunoglobulin G ligand. *Immunity*, **1**, 303–315.

SCHUCK, P. (1996) Kinetics of ligand binding to receptor immobilized in a polymer matrix, as detected with an evanescent wave biosensor. I. A computer simulation of the influence of mass transport. *Biophys. J.*, **70**, 1230–1249.

SUTOVSKY, H. & GAZIT, E. (2004) The von Hippel-Lindau tumor suppressor protein is a molten globule under native conditions: implications for its physiological activities. *J. Biol. Chem.*, **279**, 17190–17196.

SZABO, A., STOLZ, L. & GRANZOW, R. (1995) Surface plasmon resonance and its use in bio-molecular interaction analysis (BIA). *Curr. Opin. Struct. Biol.*, **5**, 699–705.

TREML, H., WOELKI, S. & KOHLER, H.-H. (2003) Theory of capillary formation in alginate gels. *Chem. Phys.*, **3**, 341–353.

YARMUSH, M. L., PATANKAR, D. B. & YARMUSH, D. M. (1996) An analysis of transport resistance in the operation of BIAcore^{TM}; implications for kinetic studies of biospecific interactions. *Mol. Immunol.*, **33**, 1203–1214.

ZHENG, Y. & RUNDELL, A. (2003) Biosensor immunosurface engineering inspired by B-cell membrane-bound antibodies: modeling and analysis of multivalent antigen capture by immobilized antibodies. *IEEE Trans. Nanobiosci.*, **2**, 14–25.